15 Feb 2022

Detonation Synthesis of Nanoscale Silicon Carbide from Elemental Silicon

Martin J. Langenderfer

Yue Zhou

Jeremy Lee Watts
Missouri University of Science and Technology, jwatts@mst.edu

William Fahrenholtz
Missouri University of Science and Technology, billf@mst.edu

et. al. For a complete list of authors, see https://scholarsmine.mst.edu/matsci_eng_facwork/2896

Recommended Citation

M. J. Langenderfer et al., "Detonation Synthesis of Nanoscale Silicon Carbide from Elemental Silicon," *Ceramics International*, vol. 48, no. 4, pp. 4456 - 4463, Elsevier, Feb 2022.
The definitive version is available at https://doi.org/10.1016/j.ceramint.2021.10.231

Ceramics International 48 (2022) 4456–4463

Contents lists available at ScienceDirect

Ceramics International

journal homepage: www.elsevier.com/locate/ceramint

Detonation synthesis of nanoscale silicon carbide from elemental silicon

Martin J. Langenderfer, Yue Zhou, Jeremy Watts, William G. Fahrenholtz, Catherine E. Johnson *

Missouri University of Science and Technology, Rolla, MO, 65409, USA

ARTICLE INFO

Keywords:
Detonation
A. Powders: Chemical preparation
B. Electron microscopy
D. SiC

ABSTRACT

Direct reaction of precursors with the products of detonation remains an underexplored area in the ever-growing body of detonation synthesis literature. This study demonstrated the synthesis of silicon carbide during detonation by reaction of elemental silicon with carbon products formed from detonation of RDX/TNT mixtures. Continuum scale simulation of the detonation showed that energy transfer by the detonation wave was completed within 2–9 μs depending on location of measurement within the detonating explosive charge. The simulated environment in the detonation product flow beyond the Chapman-Jouguet condition where pressure approaches 27 GPa and temperatures reach 3300 K was thermodynamically suitable for cubic silicon carbide formation. Carbon and added elemental silicon in the detonation products remained chemically reactive up to 500 ns after the detonation wave passage, which indicated that the carbon-containing products of detonation could participate in silicon carbide synthesis provided sufficient carbon-silicon interaction. Controlled detonation of an RDX/TNT charge loaded with 3.2 wt% elemental silicon conducted in argon environment lead to formation of ~3.1 wt% β-SiC in the condensed detonation products. Other condensed detonation products included primarily amorphous silica and carbon in addition to residual silicon. These results show that the energized detonation products of conventional high explosives can be used as precursors in detonation synthesis of ceramic nanomaterials.

1. Introduction

Detonation synthesis has evolved as a process for the industrial production of nanodiamonds that are <100 nm in diameter [1]. Detonation synthesis uses the combination of high pressure (>10 GPa) and temperature (>2000 K) of explosive detonation along with rapid quenching rates (16 billion K/s) to enable the production of metastable carbon structures such as nanodiamond. Recent research has investigated the addition of precursor materials to an explosive matrix to influence the detonation process and produce nanoscale phases not typically present in detonation products such as silicon carbide, boron nitride, and titanium carbide [2–4]. Silicon carbide nanoparticles that can be produced through detonation are used in a variety of aerospace, electrical and medical applications due to their intrinsic properties of hardness, low density, and semiconduction [5–8]. The use of explosive detonation to produce industrial nanomaterials like silicon carbide is desirable due to rapid production of the condensed metastable nanoscale phases offering potential advantages over traditional manufacturing and size reduction processes used to produce hard materials from their common thermodynamically stable phases [9,10].

Previous research demonstrated the synthesis of silicon carbide using detonation by adding polycarbosilane to a cast mixture of 1,3,5-Trinitroperhydro-1,3,5-triazine (RDX) and 2,4,6-Trinitrotoluene (TNT) [2]. Polycarbosilane is a precursor material that is pyrolyzed above 1000 °C in an oxygen-deficient environment into silicon carbide (SiC) [11]. In addition to SiC, detonation with a polycarbosilane precursor forms significant amounts of nanodiamond within the detonation products. This study is the first to evaluate the use of carbon produced by detonation itself as a precursor for the formation of SiC.

Many commonly used explosives such as TNT form free carbon during detonation due to their negative oxygen balance, or excess ratio of carbon to oxygen in the explosive [12,13]. In 1961 Urizar discovered that the detonation velocity, and ultimately detonation pressure increased linearly with increasing density of pressed TNT until it exhibited an inflection point at around 1.55 g/cm^3 where the detonation velocity inexplicably accelerated away from the linear trend [14]. This acceleration was suspected to result from a carbon phase change occurring at that density as the increase in detonation pressure caused

* Corresponding author. 1006 Kingshighway, Rolla, MO, 65409, USA.
E-mail address: catherine.johnson@mst.edu (C.E. Johnson).

https://doi.org/10.1016/j.ceramint.2021.10.231
Received 22 August 2021; Received in revised form 7 October 2021; Accepted 28 October 2021
Available online 30 October 2021

carbon to transition into the diamond or liquid forming regions of carbon phase diagram [15]. The extremely dynamic nature of detonation associated with the rapid release of energy from the detonation wave has rendered an in-depth understanding of the nature of carbon condensation within the detonation products elusive.

An on-going question is whether detonation carbon begins to coagulate and crystallize in the reaction zone before the Chapman-Jouguet condition [16], or subsequent to reaction completion, during the Taylor wave expansion, with only free carbon collisions occurring in the reaction zone, and coagulation occurring as the carbon cools across the liquid phase boundary [15]. Recent research used synchrotron illumination of the detonation wave with time resolved small angle X-ray scattering (SAXS) to image carbon condensation during detonation [13,17]. According to these studies carbon remains active after completion of the fast reaction zone with solid particle formation beginning within 100 ns of the detonation front arrival. Using SAXS, carbon growth and aggregation were also shown to occur between 100 ns and 2 μs for triaminotrintrobenzene (TATB) based compositions [17], and carbon products from RDX/TNT detonations completely stabilized by around 500 ns after the arrival of the detonation wave [13].

Carbon from detonation remains reactive and can participate in particle aggregation after the passage of the detonation wave [13,17]. This residual reactivity of carbon after the passage of detonation wave provides the opportunity for the introduction of dopants or additives such as silicon to react with the elemental carbon formed from detonation during aggregation. The conditions present in an RDX/TNT explosive detonation with the addition of elemental silicon as a post detonation reaction precursor would place the detonation products in the Si + C phase separation region of the phase diagram; however, the methodology proposed herein would allow the mixture to cool through the cubic silicon carbide forming region of the diagram as the products expand [18]. An experimental silicon-carbon phase diagram [18] is shown in Fig. 1 and is overlaid with a notional cooling path for military Composition B, a 60:40 mass ratio mixture of RDX to TNT [19]. Between the von Neumann spike and C-J state where the detonation reaction occurs, the temperatures and pressures reach 3000–3500 K and 28–40 GPa, corresponding to the Si-C immiscibility region of the phase

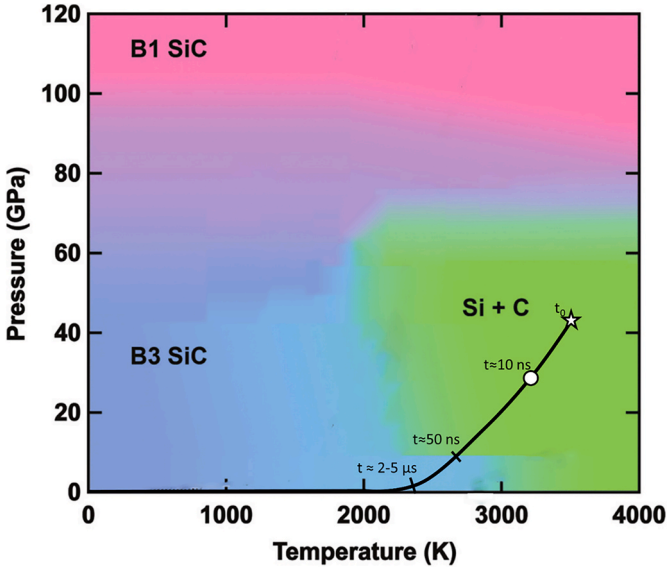

Fig. 1. Conditions produced by detonating a 60:40 mass ratio mixture of RDX and TNT from the von-Neumann spike state (43 GPA, 3500 K) indicated by a star then cooling through the Chapman-Jouguet condition (28.5 GPA, 3350 K) indicated by a circle, and into the stability region for the B3 zinc blende cubic structure of silicon carbide (Adapted from Ref. [18]). (For interpretation of the references to color in this figure legend, the reader is referred to the Web version of this article.)

diagram [20]. As the products expand and cool following detonation, temperature and pressure rapidly drop within the first 50 ns and cross into the stability region for B3 (zinc blende cubic) SiC. The pressure achieved in the detonation does not reach ~100 GPa needed to stabilize B1 (rock-salt cubic) SiC.

The present study investigated the technical feasibility of detonation synthesis of silicon carbide using elemental silicon as a precursor to react with carbon condensed from detonation of negatively oxygen balance explosives. In simulation, a charge of Composition B, a negatively oxygen balanced RDX:TNT based explosive was detonated to evaluate the evolution of temperature and pressure from the detonation through time relative to the SiC phase diagram. In experiment, a cast 150 g Si/RDX/TNT based charge was detonated in a controlled environment with the condensed products collected for phase characterization.

2. Methodology

Elemental silicon powder was added to a mixture of RDX and TNT to assess the feasibility of a direct reaction of silicon with carbon condensed from the explosive products to form silicon carbide. Morphology of the condensed phases observed in the experimental work is considered in relation to the release rate of energy from the explosive geometry predicted by a Eulerian simulation of the detonation event. A combination of X-Ray diffraction, X-Ray photoelectron spectroscopy, and high-resolution transmission electron microscopy with energy dispersive spectroscopy were used to characterize the detonation products.

2.1. Detonation simulation methodology

Composition B was simulated at the continuum scale in a 2D axisymmetric Euler domain using a Lee-Tarver Ignition and Growth reactive burn model (IGRB) in Ansys Autodyn [19]. A 60:40 RDX/TNT Composition B model was selected to develop a hydrodynamic simulation of detonation due to its similarity to the 50:50 mass ratio RDX to TNT explosive composition used in this study as well as the availability of JWL and IGRB expansion data for the explosive mixture. Pressure of the detonation products was predicted directly from the JWL equation of state, and temperature was calculated along the reference isentrope using equation (1):

$$T_{C_r}(V) = \left(\frac{V_r}{V}\right)^{\omega} T_r \tag{1}$$

where T_{Cr} is the temperature along the reference isentrope, V is the volume, V_r is the reference volume, ω is the Gruneisen coefficient, and T_r is the reference temperature [21].

The simulation was used to assess the thermodynamic state of the detonation products as a function of their expansion from the original charge geometry as the explosive detonated. An empirically determined Jones-Wilkins-Lee (JWL) equation of state modeled the expansion of the detonation products. The IGRB model of detonation allowed the assessment of the effects of charge geometry on the propagation of detonation energy by incorporating pressure dependent reaction rates through the bulk explosive charge [22].

2.2. Synthesis methodology

A mixture of 75.00 g RDX (Accurate Energetics), 75.00 g TNT (Accurate Energetics) and 5.00 g of crushed silicon (-325 mesh, Alfa Aesar), shown in Fig. 2a, was melt cast into a cylinder that was 51 mm diameter x 49 mm tall. (Fig. 2b). A 50:50 ratio of RDX to TNT was selected due to the additional free carbon available due to the higher ratio of the more negatively oxygen balanced explosive, TNT, to other more common 60:40 mixtures while maintaining pressure and temperature similar to the simulated charge. The final mass of the cast charge was 153.90 g

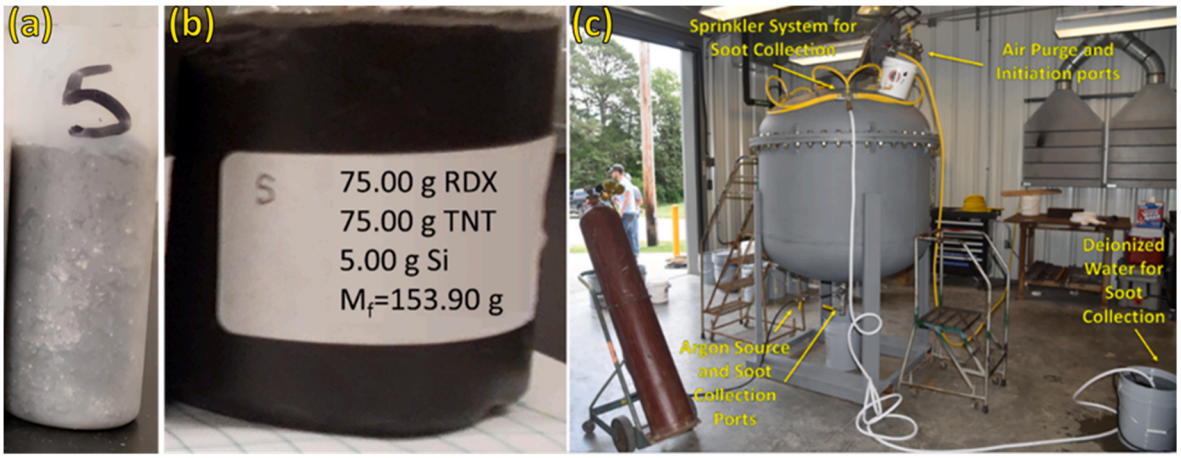

Fig. 2. Casting composition in polyethyelene molding sleeve (a), cast test charge prepared for detonation testing (b) Detonation chamber (DAVE) (c).

with 1.10 g lost due to adhesion to the molding tube during casting. One end of the charge had a 9.8 mm diameter x 12 mm deep well coaxial with the cylinder for placing the detonator. The final cast density of the charge was 1.62 g/cm^3 measured by immersion. The charge was press fit with a Teledyne Risi RP-503 exploding bridge wire detonator and suspended centrally in the 1.1 m^3 Detonation Analysis Via Extraction (DAVE) apparatus shown in Fig. 2c. The DAVE apparatus was closed, and the environment purged to less than 3 vol % oxygen by displacement of air with argon. Oxygen concentration was sampled at the bottom, center, and top of the DAVE apparatus through the purge outlet prior to testing using an Industrial Scientific Ventis Pro5 multi-gas monitor. The environment was then sealed, and the charge detonated. The condensed detonation residues were collected as a slurry using deionized water via a rinse extraction system. The condensed detonation residue was then sieved through a 100 mesh screen, decanted and dried in a vacuum oven at 100° C for further analysis.

2.3. Characterization methodology

Detonation residues were characterized using powder X-ray diffraction (XRD; Panalytical, X'Pert) analysis with Cu-Kα radiation. Scans were recorded from 5 to 90° 2θ using a step size of 0.026° and an effective count time of 0.5 s per step. Powders were also examined using transmission electron microscopy (TEM; Tecnai F20 STEM) using an accelerating voltage of 200 kV and energy dispersive spectroscopy (EDS; Oxford Instruments). Specimens for TEM were prepared by suspending 0.3 wt% soot in acetone under ultrasonic vibration for 30 min. The suspension was then deposited onto a carbon-coated 400 mesh copper grid. X-ray photoelectron spectroscopy (XPS, Kratos Axis 165) was also used for a survey elemental analysis from binding energies between 0 and 1100 eV over 500 meV steps, with a dwell time of 500 ms.

Detonation residues were dried in a vacuum oven at 100 °C and were originally analyzed in the raw unprocessed form. In addition, a 2 g sample of the detonation residue was oxidized in air at 450 °C for 24 h to remove amorphous carbon [23,24]. The oxidized residue was characterized using XRD with 0.1 wt % anatase (<325 mesh, 99.9%, Loudwolf Scientific) added as an internal standard. Rietveld refinement (RIQAS version 4.0) was used to quantify the amounts of crystalline and amorphous phases present in the detonation residue [25]. Anatase was chosen as the internal standard due to the separation of the primary identifying peaks of anatase from the primary identifying peaks of silicon and silicon carbide. The anatase used in these experiments was compared to a NIST standard (Standard Reference Material 1898, National Institute of Standards and Technology) and shown to consist of 99.97 wt% of the anatase phase of TiO_2. The raw detonation residue and air oxidized samples were further analyzed using TEM/EDS and selected area electron diffraction.

3. Results and discussion

The hydrodynamic simulation confirmed that the conditions present during RDX/TNT detonation expansion were consistent with the thermodynamic stability of SiC. The simulated products of detonation reached the C-J condition of 26 GPa and 3300 K, which was in an immiscibility region for Si and C. During expansion of the detonation products, the conditions cooled through a SiC forming region of the phase diagram before returning to ambient conditions. The condensed phase detonation products contained a mixture of carbon, silicon, amorphous SiO_2 and SiC, thus demonstrating the first synthesis of SiC by reacting elemental Si with carbon condensed from the products of a high explosive detonation.

3.1. Detonation simulations

The explosive charge geometry used in the continuum scale simulations is shown in Fig. 3a. Once initiated, the charge rapidly progressed to a peak detonation pressure of ~42 GPa at the leading edge of the wave. The steady state detonation pressure, or C-J pressure, of ~26 GPa was reached when the energy released by the detonation of the explosive generated sufficient pressure behind the wave front to drive the supersonic reaction front forward at a constant velocity [20]. While the simulated charge achieved steady state detonation, the rarefaction wave behind the detonation front did not reach a steady state due to the curvature of the detonation wave as it propagated across the 1:1 length to diameter geometry of the cylindrical charge as shown in Fig. 3b, c, and 3d. This geometry led to an expansion profile that varied with radial distance from the center of the charge and caused products to decay back to near ambient pressure conditions <1 GPa in less than 2–9 μs depending on proximity to the edge of the charge. The continuum scale model of the detonation process enabled discussion of the kinetic constraints on Si-C particle formation by predicting the pressure and temperature at various points within the environment of the detonation products as they expanded from the original condensed explosive charge geometry.

Gauge output plots from the simulated charge, shown in Fig. 4, indicated that the shock produced by the explosive detonation drove the pressure in the unreacted material to approximately 42 GPa during the von Neumann spike where the composition began to react. Following this initiating pressure spike, pressure decayed over approximately 100 ns to the Chapman-Jouguet (C-J) state at 26 GPa and 3300 K as the material completed the detonation reaction process [20]. With reaction complete, the decay of temperature and pressure varied depending on

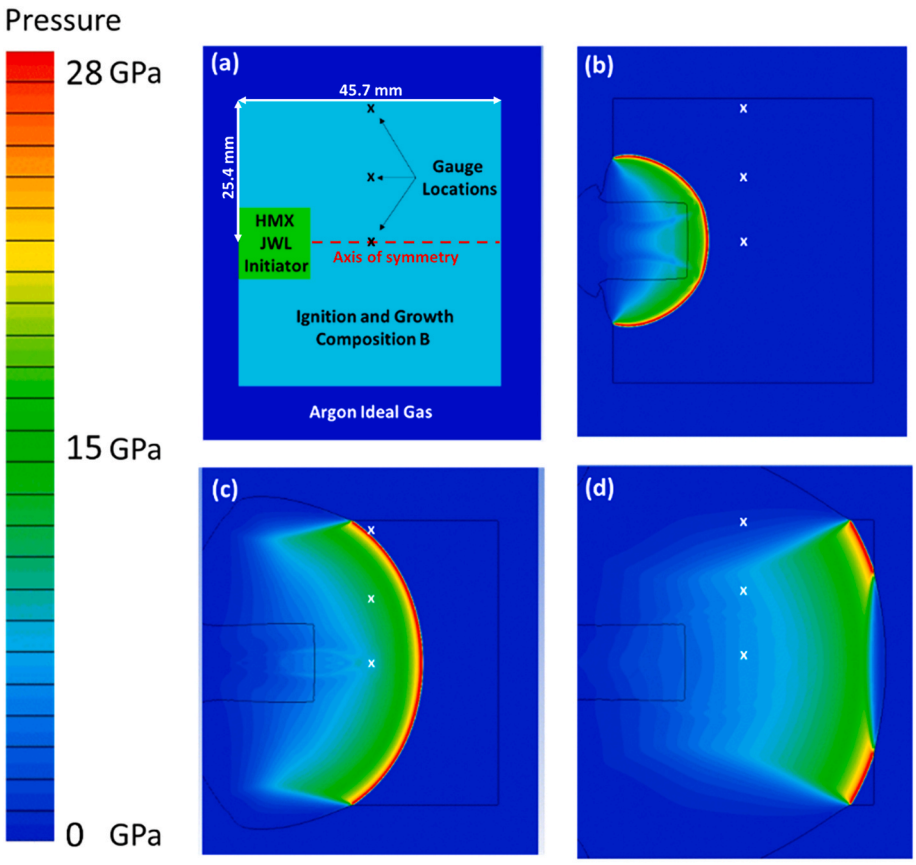

Fig. 3. Axially symmetric simulation of detonation pressure propagating through a Composition B charge geometry consistent with the geometry used in the experimental test with gauges halfway down the length of the charge at radii of 0, 12.5 and 25 mm (a) at 2 μs (b), 4 μs (c) and 6 μs (d) after charge initiation.

the expansion of the products. More confined products at the center of the charge retained higher pressure and temperature for longer periods where pressure stagnated after a short 2 μs drop from the C-J state to ~5 GPa and 2900 K for a period of ~6 μs.. These decay rates indicated that at the C-J condition, while carbon was still active for aggregation and growth, the silicon/carbon product mixture would fall in an immiscibility region of the Si-C phase diagram (i.e., silicon and carbon would be thermodynamically favorable relative to SiC), but that as pressure dropped below 10 GPa during expansion the detonation products could cool through a region of SiC stability [13,18]. These processes are likely to occur before slower oxidation of the silicon, but behind the light gas reactions of the detonation front [26]. The simulated pressure and temperature plots as a function of radial distance from the axis of the charge shown in Fig. 4 describe the duration of the detonation products in the SiC forming region of the phase diagram. The sustained temperature and pressure in the SiC forming region and densification of the products near the center of the charge a provides an increased opportunity for molecular interaction and crystal growth in comparison to the products near the edge of the charge, which expand and dissociate more rapidly; however, the more rapid drop in pressure near the edge of the charge may be beneficial to the production of SiC. These findings necessitate an experimental study of the function of charge diameter on product confinement to relate the quantity of SiC observed in the products to the time that the pressure and temperature remain within the SiC stability region.

3.2. SiC synthesis

The crystalline silicon liquified by the detonation shock was anticipated to react with carbon as the carbon condensed from the detonation product flow resulting in the production of SiC [27,28]. Silicon was also anticipated to oxidize during product expansion resulting in amorphous SiO_2 production. The detonation soot was also anticipated to contain residual crystalline Si that had been added as a precursor as well as sp^2, sp^3, and amorphous carbon soot typical of RDX/TNT detonations. The total mass of condensed detonation residue collected after drying was 12.03 g. X-ray diffraction patterns of the raw unprocessed soot, shown in Fig. 5, exhibited a broad peak centered around 24° indicative of amorphous carbon and/or SiO_2. Crystalline silicon (PDF card 01-075-0589) was indicated by sharp peaks at 28.4°, 47.3°, 56.1°, 69.0 and 88.0° corresponding to the (111), (220), (311), (400), and (422) Miller indices of the Si diamond cubic lattice. In addition, broad peaks at 36°, 41° 60°, 72°, and 75° were observed corresponding to the (111), (200), (220), (311), and (222) Miller indices associated with the cubic structure of β-SiC (PDF card 01-073-1708).

After 24 h of air oxidation at 450 °C the mass of the carbon soot sample reduced by 49% and its color changed from black to light grey as shown in Fig. 6. XRD patterns of the oxidized detonation residue showed decreases in the intensity of the broad peaks centered around 27° and 43°. The reduction in peak intensity indicates removal of amorphous carbon, but retention of crystalline peaks for Si and SiC. Amorphous carbon was apparently removed by oxidation between 400 °C and 450 °C, which is consistent with other reports [23].

Rietveld refinement of XRD patterns for unpurified and air oxidized specimens containing an internal standard are shown in Fig. 7. The unprocessed detonation residue contained 4.3 wt% elemental silicon and 3.1 wt% β-SiC with 92.6 wt% amorphous content. The air oxidized sample was shown to contain 8.8 wt% elemental silicon and 7.1 wt% β-SiC with amorphous content reduced to 84.1 wt% due to the oxidation of carbon. The goodness of fit for the Rietveld refinement is indicated by R_{wp} values of 4.61 and 3.95 respectively for the raw soot, and the oxidized sample. The doubling in concentration of SiC and Si after

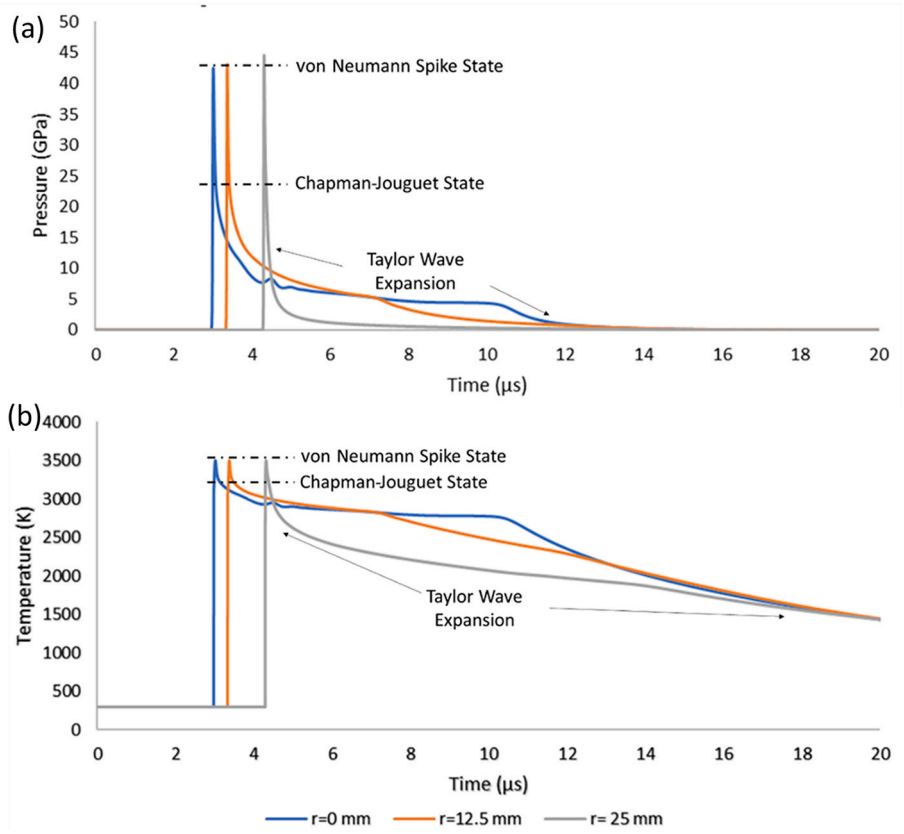

Fig. 4. Plots of simulated detonation pressure (a) and temperature (b) measured at simulated gauge location during detonation and expansion predicted by JWL equation of state at varying radii from the center of the charge corresponding to gauge points shown in Fig. 3.

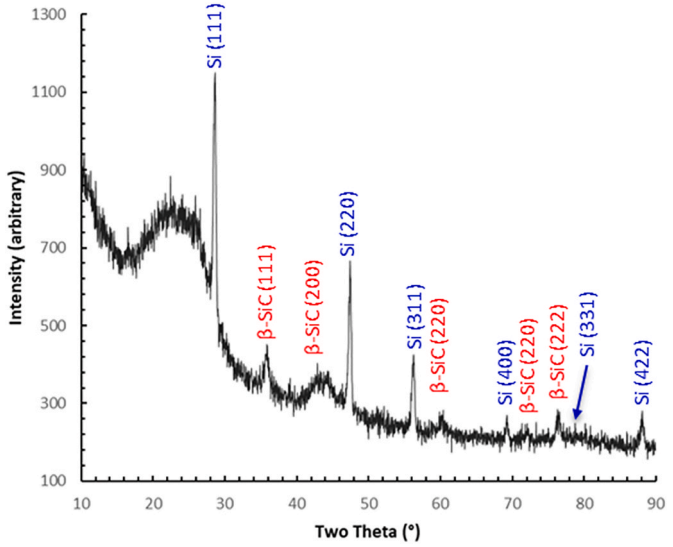

Fig. 5. XRD pattern of the raw unpurified detonation residue with labeled peaks for crystalline silicon and SiC. (For interpretation of the references to color in this figure legend, the reader is referred to the Web version of this article.)

oxidation showed good agreement with the relative peak intensity despite a 49% reduction in mass after oxidation in air. This analysis revealed that the overall concentration of β-SiC could be estimated at 3.1 wt % for an overall estimated yield in the collected raw detonation products of 0.4 g.

The unprocessed and air oxidized detonation residues were analyzed via XPS and the results are shown in Table 1. The 120% and 130% increase in the atomic concentrations of Si and O respectively after oxidation showed good agreement with the 105% and 129% increase in elemental Si and β-SiC weight concentrations observed through XRD analysis. XPS indicated that the most notable change after oxidation was reduction of the C1s peak, which decreased by ~74%. The loss of amorphous carbon is consistent with XRD analysis that showed reduction of the broad peaks at 27° and 43°.

TEM analysis revealed a mixture of both amorphous and crystalline material in the dried, but unprocessed detonation residues. Spherical SiO_2 particles greater than 500 nm in diameter were observed in the residue as shown in Fig. 8a. Near the spherical SiO_2 particles, polycrystalline agglomerates (Fig. 8b) of polyhedral particles less than 50 nm in diameter were observed that were suspected as a mixture of Si and SiC. The abundance of amorphous carbon within the raw detonation residue encapsulated the crystalline particles present obscuring the view for high resolution imaging of individual particles (Fig. 8c). Initially the excess carbon precluded the observation of definitive identifying characteristics of SiC through SAED or EDS, which prompted the use of purification techniques to remove excess carbon from the sample and obtain high resolution images of the individual crystals.

Imaging of the oxidized residue revealed the presence of agglomerated crystalline particles (Fig. 9a) abundant in the residue. The residue was largely free of amorphous carbon, which enabled clear high-resolution imaging of individual crystalline particles, shown in Fig. 9b. The crystalline particles had several defining features of crystalline silicon carbide. An image taken along the [110] zone axis in Fig. 9b showed visible stacking faults along the {111} planes with an interplanar spacing of 2.5 Å. Additionally, double spotting and streaking observed in the SAED along the [110] zone axis along the <111> direction indicated significant random stacking in the {111} family of planes. Complementary compositional information collected by EDS,

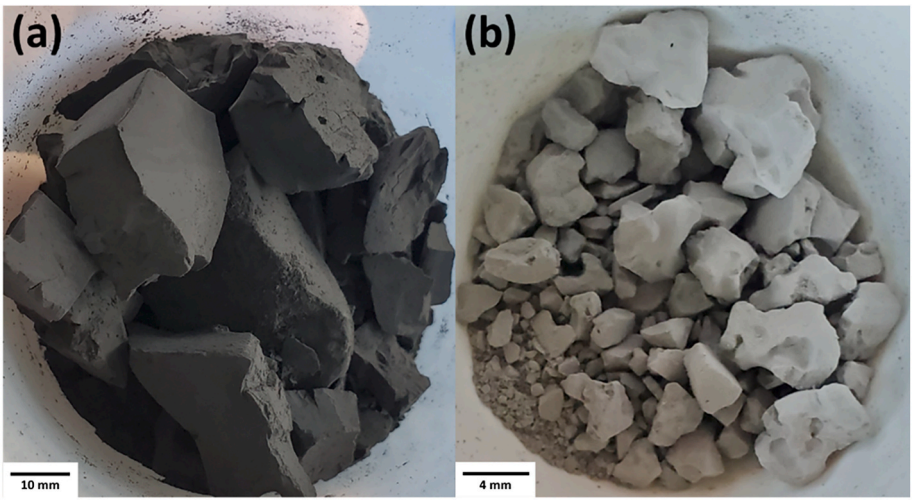

Fig. 6. Silicon loaded RDX/TNT detonation residue before (a) and after (b) 24 h air oxidation at 450 °C. (For interpretation of the references to color in this figure legend, the reader is referred to the Web version of this article.)

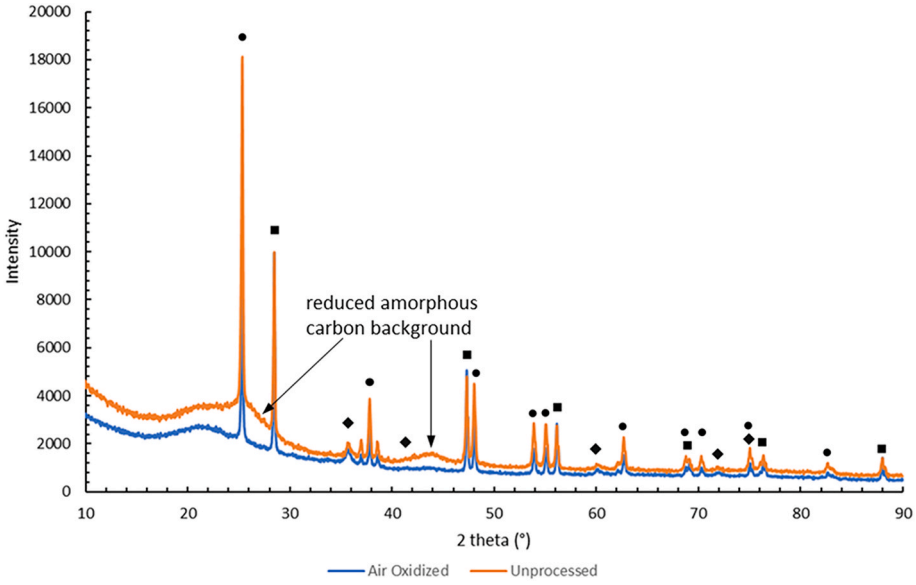

Fig. 7. XRD pattern of the unprocessed residue (orange) compared to the air oxidized residue at 450 °C (blue) with marked peaks for anatase internal standard (TiO2,●), Si (■), and β-SiC (◆). (For interpretation of the references to color in this figure legend, the reader is referred to the Web version of this article.)

Table 1
Surface Elemental analysis quantification from XPS.

	Unprocessed		Air Oxidized	
	At. %	Wt. %	At. %	Wt. %
Si 2p	15.6	27.4	36.1	65.3
C 1s	60.8	47.0	14.8	11.4
N 1s	1.3	1.2	N/A	N/A
O 1s	22.2	24.3	49.0	53.6

indicated that the imaged particle consisted of 61 atomic percent (at. %) Si, 31 at.% C and 3 at.% O. Analysis also found 7 at. % Cu was observed resulting from the Cu sample grid. The Si to C ratio could be affected by the presence of additional Si in the particles, but is more likely an artifact of the lower energy of the C characteristic x-rays compared to x-rays from Si, which would result in a lower sampling volume for C compared to Si and correspondingly lower detected amount of C [29]. Taken together, the observed interplanar spacings and stacking faults coupled with the cubic structure observed in SAED and compositional information by EDS confirmed the presence of crystalline β-SiC in the detonation residues [29].

Both XRD and TEM analyses indicate that β-SiC nanoparticles were produced by the detonation process. In addition, thermal oxidation was effective in removing the amorphous carbon in the residue, which facilitated the characterization. For industrial purposes, the remaining elemental Si could also be oxidized at temperatures approaching 900 °C after which remaining SiO_2 could be dissolved through boiling in hydrofluoric acid leaving behind only crystalline β-SiC nanopowders suitable for use in industrial applications [23,30,31,32]. This level of intensive processing, however, was beyond the scope of the present study that had the goal of demonstrating the feasibility of forming SiC by reacting a silicon powder precursor with carbon from detonation without requiring polymeric SiC precursors to be incorporated into the explosive matrix [2].

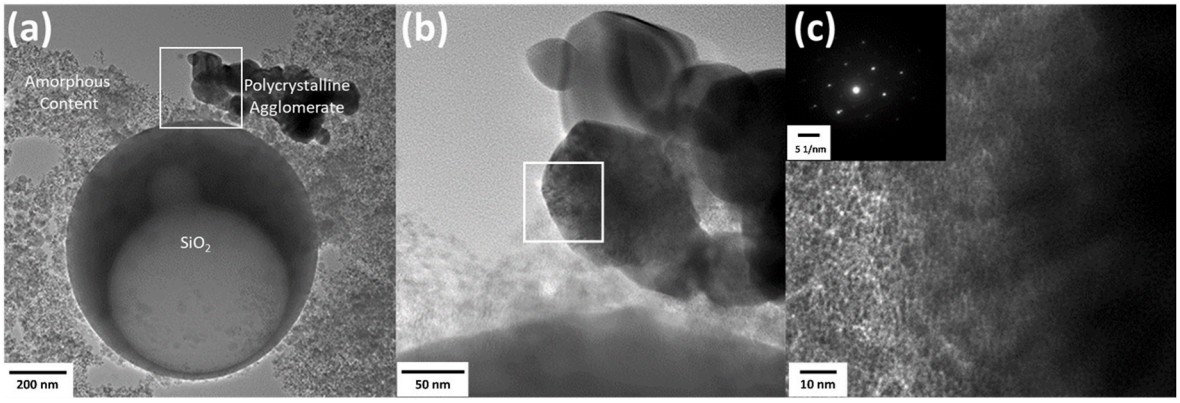

Fig. 8. TEM images of the raw unpurified detonation residue showing amorphous SiO2, near agglomerated Si/SiC clusters (a), obscured in high resolution imaging at greater magnification by an amorphous carbon coating (b and c).

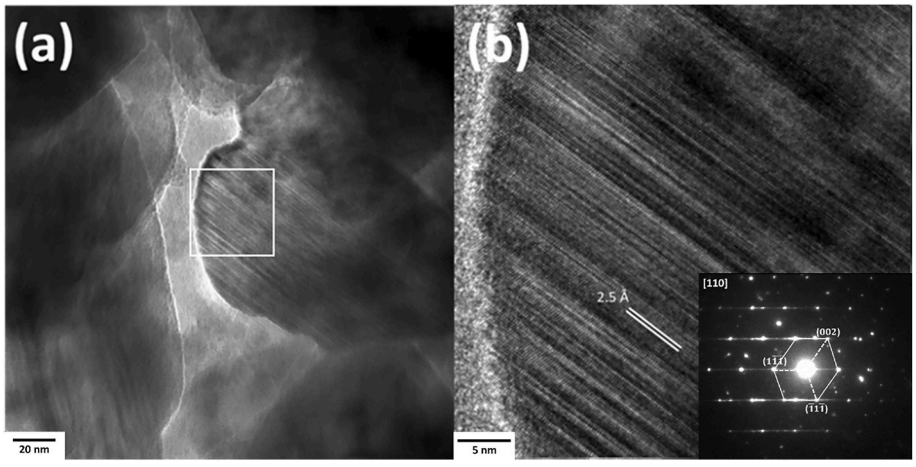

Fig. 9. High resolution TEM images of SiC in detonation residue after 24 h oxidation at 450 C (a) showing clearly defined stacking faults and cubic structure of β-SiC.

4. Future works

This study demonstrated the possibility of SiC nano powder production by reacting carbon liberated by TNT detonation with elemental silicon particles added to the explosive. During the study, several potential opportunities for improvement in product yield and SiC concentration were identified. One of the most important areas identified for further optimization of the process is extending the conditions for Si to react with C during detonation product expansion. This optimization can be pursued through a variety of methods.

First, increasing the carbon concentration in the detonation products would increase the degree of atomic interaction, which could potentially increase SiC formation. This can be accomplished by decreasing the ratio of RDX:TNT thus decreasing the oxygen balance and producing more carbon from the detonation. These changes will also affect the detonation performance of the explosive in terms of pressure and temperature, which must also be further evaluated. Second, increasing the silicon concentration in the detonation products could provide more interaction with carbon as long as the detonation produces SiC forming conditions. Simulations indicated that radial confinement of the products would affect the evolution of T and P during product expansion, which could extend the duration in the SiC forming region. A parameterized study could evaluate the effect of charge diameter on SiC production. Finally, concurrent studies have shown that particle size affects degree of product formation observed during detonation, likely due to differences in transient thermal conduction [25]. A study is needed to evaluate the role of reactive additive particle size on the yield of desirable detonation products such as SiC.

5. Conclusions

Detonation synthesis of silicon carbide nanoparticles was demonstrated by reacting carbon condensed from an RDX/TNT detonation with elemental silicon incorporated into an explosive charge. The presence of β-SiC in the post detonation residue was indicated by XRD and confirmed through TEM analysis with selected area electron diffraction and energy dispersive spectroscopy. X-ray photoelectron spectroscopy revealed that oxidation removed amorphous carbon from the detonation residue. The estimated yield of β-SiC in the 12.025 g of collected detonation residue was 3.1 wt% from a 153.90 g charge composed of a 50:50 mass ratio RDX/TNT detonation and containing 5.00 g of uniformly added silicon. Most of the detonation products consisted of amorphous carbon and SiO_2, which can both be removed from the detonation residue through either thermal oxidation or acid purification treatments [23,30,31]. These results along with an Eulerian hydrodynamic model of the detonation wave propagation showed that the pressures and temperatures associated with RDX/TNT detonation would initially fall in an Si/C immiscibility region of the phase diagram, but would cool through a β-SiC forming region before the oxidation of elemental silicon, and while the detonation carbon was chemically reactive within 1 μs of the passage of the detonation wave [13,26].

The implication of this work is that the addition of precursors like elemental silicon can be used to produce β-SiC nanoparticles through reaction with carbon liberated by detonation. This work shows that

elemental precursors can react with detonation products to selectively form desired phases. The proposed methodology requires optimization and further testing to assess the effect of the amount and particle size of the precursor on the balance between detonation product formation and the detonation velocity and pressure of the explosive. However, this study shows promise of explosive detonation to produce desired nano sized ceramic phases from the carbon of detonation when reacted with elemental precursor additives.

Declaration of competing interest

The authors declare that they have no known competing financial interests or personal relationships that could have appeared to influence the work reported in this paper.

Acknowledgements

This research was supported by the Synthesis and Processing of Materials program in the Army Research Office as project W911NF-18-1-0155. The Rock Mechanics and Explosives Research Center as well as the Advanced Materials Characterization Laboratory, namely Dr. Eric Bohannan were instrumental to the completion of this research both through the development of the Rietveld Refinement model used in this study as well as the instrumentation and analysis performed with XRD and XPS. Thanks to Dr. Vadym Mochalin for insights into the mechanisms of detonation synthesis.

References

[1] V.U. Dolmatov, M.V. Veretennikova, V.A. Maruchkov, V.G. Sushchev, Currently available methods of industrial diamond synthesis, Phys. Solid State (2004) 596–600.
[2] M.J. Langenderfer, W.G. Fahrenholtz, S. Chertopalov, Y. Zhou, V.N. Mohcalin, C. E. Johnson, Detonation synthesis of silicon carbide nanoparticles, Ceram. Int. 46 (5) (2020) 6951–6954.
[3] S. Ghosh, P. Ranjan, A. Kumaaar, R. Sarathi, S. Ramaprabhu, Synthesis of nanometer titanium carbide by detoantion shock wave, Explos. Shock Waves 40 (9) (2020).
[4] M. Ornek, K.M. Reddy, C. Hwang, V. Domnich, A. Burgess, S. Pratas, J. Calado, K. Y. Xie, S.L. Miller, K.J. Hemker, R.A. Haber, Observations of explosion phase boron nitride formed by emulsion detonation synthesis, Scripta Mater. 145 (2018) 126–130.
[5] S.E. Saddow, Silicon Carbide Biotechnology, Elsevier, Waltham, MA, 2012.
[6] D.G. Senesky, B. Jamshidi, K.B. Cheng, A.P. Pisano, Harsh environment silicon carbide sensors for health and perfomance monitoring of aerospace systems: a review, IEEE Sensor. J. 9 (11) (2009) 1472–1478.
[7] S.V. Zhitnyuk, N.A. Makarov, T.V. Guseva, New silicon carbide based ceramic armor materials, Glass Ceram. 71 (2014) 6–9.
[8] P. Gibot, L. Vidal, L. Laffont, J. Mory, Zirconia nanopowder synthesis via detonation of trinitrotoluene, Ceram. Int. 46 (17) (2020) 27057–27062.
[9] N. Luo, K.X. Liu, X. Li, H. Shen, S. Wu, Z. Fu, Systematic study of detonation synthesis of ni based nanoparticles, Chem. Eng. J. 210 (2012) 114–119.
[10] T. Wang, W. Gong, X. He, Z. Kou, G. Tan, S. Zhou, H. Yu, M. Fan, H.H. Kung, Synthesis of highly nanoporous β-silicon carbide from corn stover and sandstone, ACS Sustain. Chem. Eng. 8 (39) (2020) 14896–14904.
[11] G.D. Soraru, F. Babonneau, J.D. Mackenzie, Structural evolutions from polycarbosilane to SiC ceramic, J. Mater. Sci. 25 (1990) 3886–3893.
[12] V.N. Mochalin, O. Shenderova, D. Ho, Y. Gogotsi, The properties and applications of nanodiamonds, Nat. Nanotechnol. 7 (2012) 11–23.
[13] M. Bagge-Hansen, S. Bastea, J.A. Hammons, M.H. Nielsen, L.M. Lauderbach, R. L. Hodgin, P. Pagoria, C. May, S. Aloni, A. Jones, W.L. Shaw, E.V. Bokovsky, N. Sinclair, R.L. Gustavsen, E.B. Watkins, B.J. Jensen, D.M. Dattelbaum, M. A. Firestone, R.C. Huber, B.S. Ringstrand, J.R.I. Lee, T. van Buuren, L.E. Fried, T. M. Willey, Detonation synthesis of carbon nano-onions via liquid carbon condensation, Nat. Commun. 10 (2019) 3819.
[14] M.J. Urizar, E. James Jr., L.C. Smith, Detonation velocity of pressed TNT, Phys. Fluid. 4 (1961) 262–274.
[15] J.A. Viacelli, F.H. Ree, Carbon particle phase transformation kinetics in detonation waves, J. Appl. Phys. 88 (2000) 683–690.
[16] C.M. Tarver, L.E. Fried, A.J. Ruggiero, D.F. Calef, Energy transfer in solid exposives, in: Detonation Symposium, 1993. Boston, MA.
[17] E.B. Watkins, K.A. Velizhanin, D.M. Dattelbaum, R.L. Gustavsen, T.D. Aslam, D. W. Podlesak, R.C. Huber, M.A. Firestone, B.S. Ringstrand, T.M. Willey, M. Bagge-Hansen, R. Hodgin, L. Lauderbach, T. van Buuren, N. Sinclair, P.A. Rigg, S. Seifert, T. Gog, Evolution of carbon clusters in the detonation products of the triaminotrinitrobenzene (TATB)-Based explosive PBX 9502, J. Phys. Chem. 121 (41) (2017) 23129–23140.
[18] K. Daviau, K.M. Lee, Decomposition of Silicon Carbide at high pressures and temperatures, Phys. Rev. B 96 (17) (2017), 174102.
[19] M.J. Murphy, E.J. Lee, A.M. Weston, A.E. Williams, Modeling shock initiation in composition B, in: Detonation Symposium, Mass, Boston, 1993.
[20] P. Cooper, Explosives Engineering, Wiley, New York, 1996.
[21] R. Menikoff, JWL Equation of State, Los Alamos National Lab, Los Alamos, NM, 2017.
[22] E.L. Lee, C.M. Tarver, Phenomenological model of shock initiation in heterogeneous explosives, Phys. Fluid. 23 (1980) 2362.
[23] V. Pichot, M. Comet, E. Fousson, C. Baras, A. Senger, F. Le Normand, D. Spitzer, An efficient purification method for detoantion nanodiamonds, Diam. Relat. Mater. 17 (1) (2008) 13–22.
[24] S. Osswald, G. Yushin, V. Mochalin, S.O. Kucheyev, Y. Gogotsi, Control of sp2/sp3Carbon ratio and surface chemistry of nanodiamond powders by selective oxidation in air, J. Am. Chem. Soc. 128 (35) (2006) 11635–11642.
[25] M. Langenderfer, W.G. Fahrenholtz, J. Heniff, L. Nguyen, J. Watts, C.E. Johnson, Shock focusing effects on silica phase production during cyclotrimethylene trinitramine/2,4,6-trinitrotoluene detonations, J. Appl. Phys. 129 (2021).
[26] P.E. Anderson, P. Cook, A. Davis, K. Mychajlonka, M. Mileham, Silicon fuel in high performance exploives, Propellants, Explos. Pyrotech. 39 (1) (2014) 74–78.
[27] C.C. Yang, L.Q. Jiang, Temperature-Pressure phase diagram of silicon determined by Clapeyron equation, Solid State Commun. 129 (7) (2004) 437–441.
[28] C.C. Yang, J.C. Li, Q. Jiang, Temperature-pressure phase diagram of silicon determined by Clapeyron equation, Solid State Commun. 129 (7) (2004) 437–441.
[29] A.N. Dorner, D.J. Barton, Y. Zhou, G.B. Thompson, G.E. Hilmas, W.G. Fahrenholtz, Solute distributions in tantalum-containing zirconium diboride ceramics, J. Am. Ceram. Soc. 103 (4) (2020) 2880–2890.
[30] Q. Xu, Z. Peipei, S. Qingyun, R. Tu, M. Yang, S. Zhang, L. Zhang, T. Goto, J. Yan and S. Li, "Elimination of Double Position Domains in Epitaxial <111> 3C-SiC on Si (111) by Laser CVD".
[31] J.X. Zhang, K. Hoshino, Fundamentals of nano/microfabrication and scale effect, in: Molecular Sensors and Nanodevices, second ed., Academic Press, 2019, pp. 43–111.
[32] R.C. Gehringer, Method for Hydrofluoric Acid Digestion of Silica/alumina Matrix Material for the Production of Silicon Tetrafluoride, Aluminum Fluoride and Other Residual Metal Fluorides and Oxides, United States of America Patent US5242670A, 07 09 1993.